

Chapter 2

Theory of Lidar

2.1 Introduction

This chapter introduces the subject of light scattering by molecules and water droplets in the atmosphere and gives an overview of the theory essential for interpreting elastic lidar returns from clouds and aerosols. First, parameters describing droplet size distributions in clouds are explained. Following this, scattering, extinction, and the relationship between the two are considered. Then the elastic backscatter lidar equation is introduced and the derivation of a standard signal inversion method, commonly referred to as the Klett inversion, is given, along with some discussion of its strengths and shortcomings. Finally, an expression for attenuated backscatter, the range-corrected calibrated signal, is given for use in comparison of measurements from different instruments.

2.2 Composition of Liquid Clouds

Because the nature of the particles that constitute a cloud determines the way light will interact with it, it is important to consider cloud composition when probing with lidar. Cloud properties have been studied extensively through active and passive remote sensing techniques, in situ measurements, and modelling [1]. This knowledge, in the form of cloud droplet size distributions and particle concentrations, for example, can be used to model how light is scattered by a cloud and predict return signals that might be detected from it. This is important for the current work particularly because water clouds with well understood droplet properties can be used for ceilometer attenuated backscatter calibration as explained later in this chapter and applied in Chap. 5.

A typical approach to modelling cloud droplet sizes is to consider spherical droplets with the gamma type distribution function, $f(a)$, described by Deirmendjian such that [2]

$$f(a) = \frac{\mu^{\mu+1} a^\mu e^{-\mu \frac{a}{a_0}}}{\Gamma(\mu + 1) a_0^{\mu+1}} \quad (2.1)$$

where a is a random variable representing droplet radius, a_0 is the mode of the distribution, and μ describes the width of the distribution and can be expressed as

$$\mu = \frac{1}{C_\sigma^2} - 1, \quad (2.2)$$

in which C_σ is the coefficient of variance. Note that the function $\Gamma(x)$ is the gamma function [3]

$$\Gamma(x) = \int_0^\infty e^{-t} t^{x-1} dt, \quad (2.3)$$

which for integer values of x can be calculated as a factorial such that

$$\Gamma(x + 1) = x! \quad (2.4)$$

Often the parameter used to describe the droplet size distribution is the effective radius, a_{eff} , where [4]

$$a_{\text{eff}} = \left(1 + \frac{3}{\mu}\right) a_0. \quad (2.5)$$

For water clouds the mode, a_0 , ranges from 4 to 20 μm [5], and μ ranges from 2 to 8, which produces an effective radius range of 5–50 μm [4]. According to Han et al., however, a_{eff} typically ranges from 5 to 15 μm [6].

The C1 distribution of Deirmendjian [2], commonly used to model the droplet size distribution of cumulus clouds in the literature, uses the values $a_0 = 4 \mu\text{m}$ and $\mu = 6$ in Eq. 2.1. This yields an effective radius of $a_{\text{eff}} = 6 \mu\text{m}$. Fomin and Mazin [7] caution that when relating model to measurement it is important to consider that the width of the droplet size distribution typically increases with the volume of the sampling region. They suggest that a value of $\mu = 6$ only applies to small spatial averaging regions.

Figure 2.1 shows an example of close agreement between measured and modelled distributions. Here the results of an in situ measurement of droplet size distribution using a forward scattering spectrometer probe 500 m above the base of a continental cumulus cloud given by [8] were extracted from the original data and plotted alongside the modelled C1 distribution.

A comprehensive discussion of the formation and makeup of liquid water, mixed phase, and ice clouds is beyond the scope of this work. Understanding these properties and processes is an important area of research, however, both in terms of simulation and inversion of lidar returns, and in terms of improving understanding of radiative

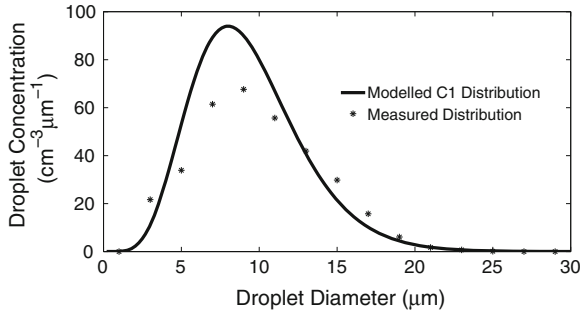


Fig. 2.1 Droplet diameter distribution measured 500m above cloud base in continental cumulus in Northern Colorado, USA, with a measured number density $N = 780 \text{ cm}^{-3}$, as reported by Knollenberg [8] compared with the C1 distribution at the same number density

processes in clouds. These subjects are considered in detail in works by Pruppacher and Klett [1], Hobbs and Deepak [9], and Lynch et al. [10].

2.3 Elastic Scattering and Transmission of Light in the Atmosphere

Elastic interaction of light with scatterers is typically described by one of two processes, depending upon the size of the scatterers. Rayleigh scattering is used to describe scattering in situations where the scatterer is very small compared to the wavelength of the light. Mie scattering is typically used to describe interactions of light with particles whose sizes are similar to or somewhat larger than the wavelength of the light. Note that single-scattering, in which a photon interacts with one scatterer only before being detected, is typically the dominant process measured by lidar. However, multiple scattering, in which a photon interacts with more than one scatterer before being detected, must often be considered, particularly in systems with large fields of view.

2.3.1 Rayleigh Scattering

Scattering by gas molecules in the atmosphere can be described by Rayleigh scattering. As expressed by Kovalev and Eichinger [11], the wavelength-dependent molecular volume backscatter coefficient β_m can be determined such that

$$\beta_m = \frac{8\pi^3(m^2 - 1)N}{3N_s^2\lambda^4}, \quad (2.6)$$

where m is the real part of the refractive index, N is the molecular number density at the pressure and temperature of the scattering volume, N_s is the molecular number density at standard temperature and pressure ($2.547 \times 10^{19} \text{ cm}^{-3}$ at 288.15 K and 101.325 kPa), and λ is the wavelength of the light. Rayleigh scattering is symmetric for forward scattered and backscattered light. At sea level the molecular volume backscatter coefficient can be calculated as [11]

$$\beta_m = 1.39 \left[\frac{550}{\lambda(\text{nm})} \right]^4 \times 10^{-8} \text{ cm}^{-1} \text{ sr}^{-1}. \quad (2.7)$$

The most significant factor in these expressions is the λ^{-4} wavelength dependence of the scattering intensity which means, for example, that ultraviolet light at 355 nm is scattered 81 times more strongly by the molecular atmosphere than near-infrared light at 1,064 nm. Note that while scattering by very small particles is in fact Rayleigh scattering, in lidar research the term Rayleigh scattering usually refers only to scattering from the molecular atmosphere [12].

2.3.2 Mie Scattering

When the scatterer size is similar to the wavelength of incident light, a theory developed by Gustav Mie in 1908 [13] can be used to calculate the scattering phase function for spherical, optically conducting particles. In this case the scattering is given by an infinite series expansion.

Some example scattering phase functions calculated by a Mie-based method [14] at a wavelength of 1 μm for spheres of various radii with refractive index 1.5 are shown in Figs. 2.2 and 2.3. As shown in Fig. 2.2, when the radius is 0.1 μm , ten times smaller than the wavelength, the forward and backward scattering distributions are similar to each other. Note that when the radius is decreased to 0.01 μm , the forward and backward scattering distributions become essentially symmetric and approach the Rayleigh scattering solution.

As the particle radius increases with respect to the wavelength, the distribution becomes more pointed in the forward direction. Figure 2.3 shows the scattering distribution for radius equal to wavelength. A close-up view around the origin shows scattering lobes at various angles, the position and intensity of which relate to interference patterns of light propagating around and through the sphere; these will vary from the theory for non-spherical shapes and imperfect optical conductor materials [11]. As the size of the sphere increases further, Mie theory gives larger and larger forward scattering lobes until the sphere is significantly larger than the wavelength of the light, at which time geometric optics [15] can be used to describe the light path. Note that Deirmendjian [2] used Mie theory to calculate scattering phase functions for C1 and other droplet size distributions, thus providing a reference that has been used, for example, to calculate multiple scattering effects in clouds [16].

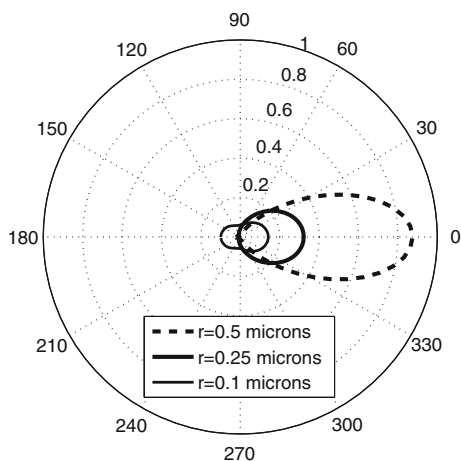


Fig. 2.2 Relative scattering intensity of $1\text{ }\mu\text{m}$ wavelength light by spherical particles of refractive index 1.5 as a function of angle (in degrees) for three different radii considering light entering from the *left*

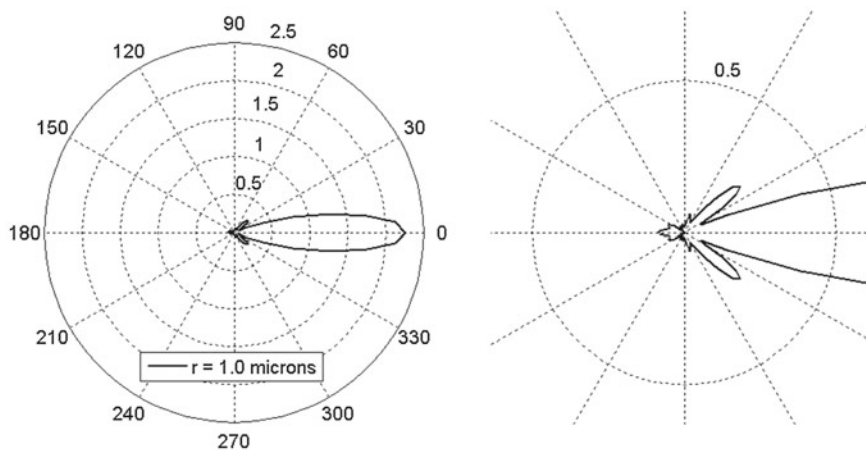


Fig. 2.3 Relative scattering intensity of $1\text{ }\mu\text{m}$ wavelength light by spherical particles of refractive index 1.5 as a function of angle (in degrees) for particles of $1\text{ }\mu\text{m}$ radius considering light entering from the *left*. A close-up view around the origin is shown on the *right*

2.3.3 Transmission and Extinction

The transmission and extinction of light travelling through the atmosphere are key considerations for lidar. They are explained here following the approach of Kovalev and Eichinger [11].

For a given wavelength, the transmittance $T(H)$ of a layer of thickness H can be expressed as the ratio of the outgoing radiant flux F to the incoming radiant flux F_0 such that

$$T(H) = \frac{F}{F_0}. \quad (2.8)$$

$T(H)$ ranges from 0 for a fully-attenuating medium to 1 for a medium through which all of the light passes without experiencing any scattering or absorption. In order to account for range-variable transmission through a heterogeneous medium, the extinction coefficient function $\alpha(r)$ is introduced to describe, for each differential range element dr , the probability of photon scattering or absorption per unit path length. The change in radiant flux over a differential element can be considered as a function of $\alpha(r)$ such that

$$dF(r) = -\alpha(r)F(r)dr. \quad (2.9)$$

From this expression the Beer-Lambert-Bouger law, which relates outgoing to incoming radiant flux, can be derived such that

$$F = F_0 e^{-\int_0^H \alpha(r)dr}, \quad (2.10)$$

and by substituting Eq. 2.8 into Eq. 2.10 the transmittance can then be expressed as

$$T(H) = e^{-\int_0^H \alpha(r)dr}. \quad (2.11)$$

Here the integral in the exponent $\int_0^H \alpha(r)dr$ is the summed extinction along the path and is therefore used to express the optical depth τ_α .

If inelastic scattering is sufficiently small to be disregarded as is usually the case for elastic lidar, the extinction coefficient can be expressed as the sum of the total elastic scattering coefficient, $\beta_T(r)$, and the absorption coefficient, $\alpha_A(r)$, such that

$$\alpha(r) = \beta_T(r) + \alpha_A(r). \quad (2.12)$$

For a cloud lidar, liquid water droplets are the primary particles of interest. The complex refractive index of water (the real part of which is approximately 1.33), which can be used to determine its scattering and absorption properties for a given radius, has been measured over a wide range of wavelengths by various authors, for example, by Hale and Querry [17]. However, total absorption and scattering vary with size and concentration of scatterers, which may not be known, and soluble aerosols dissolved in water may add complexity to light-particle interactions by increasing the imaginary part of the refractive index, i.e. absorption. In addition, the presence of mixed particle types in a scattering volume may introduce further complexity. This means it can be very difficult to separate the constituents of the extinction coefficient. Nonetheless, by applying some assumptions about the

atmosphere and/or by including information from external measurements, it is possible to draw some conclusions about the relationship between total extinction and backscatter, a relationship that is of key importance to lidar measurements.

2.3.4 The Lidar Ratio

Interpreting the physical meaning of a measured lidar signal is an inverse problem. Inversion techniques must therefore be applied in order to determine optical properties of atmospheric constituents from which return signals are collected. From an elastic lidar measurement of range-resolved power, it is not possible to distinguish with certainty the contributions of the two variables, extinction and backscatter, to the signal profile because the relationship between the range-dependent backscatter coefficient $\beta(r)$ and the range-dependent extinction coefficient $\alpha(r)$ varies depending upon the content of the measurement volume at each range r . Consider, for example, that a return from a thin, diffuse, weakly scattering cloud layer with clear air between it and the lidar instrument could look very similar to a return from thin, dense, strongly scattering cloud layer with a strongly absorbing gas layer between it and the lidar. In order to account for these differences, the range-dependent backscatter to extinction ratio $\Pi_p(r)$ can be expressed [11]

$$\Pi_p(r) = \beta(r)/\alpha(r). \quad (2.13)$$

This expression can be useful for applying assumptions to the lidar ratio over the detection range if, for example, $\Pi_p(r)$ is assumed to be constant or a linear function, or if it can be calculated using a model or measured by some method.

Klett explained that the relationship between backscatter and extinction can be also be approximately expressed in the form [18]

$$\beta(r) = B_0 \alpha^k(r), \quad (2.14)$$

where B_0 and k are assumed to be constants. This power law expression was used in differential form in Klett's original derivation of the backward inversion method. He noted that k is wavelength-dependent and also influenced by aerosol properties in the measurement volume and explained that it is typically in the range of $0.67 \leq k < 1.0$.

The lidar ratio is a fundamental unknown for most elastic lidar measurements. The quality of elastic lidar inversion often depends on the accuracy of the assumptions made regarding the lidar ratio.

2.4 Elastic Lidar System Constant

A number of parameters of a lidar system that affect the measured level of backscattered light are typically factored into a system constant, K_s , expressed by Wandinger [12] such that

$$K_s = P_0 \frac{c\tau}{2} A_0 \eta. \quad (2.15)$$

Here P_0 is the average laser power output during a pulse, c is the speed of light, τ is the laser pulse duration, A_0 is the area of the receiver objective as shown in Fig. 2.4, and η is the total efficiency of the instrument's optical path multiplied by the

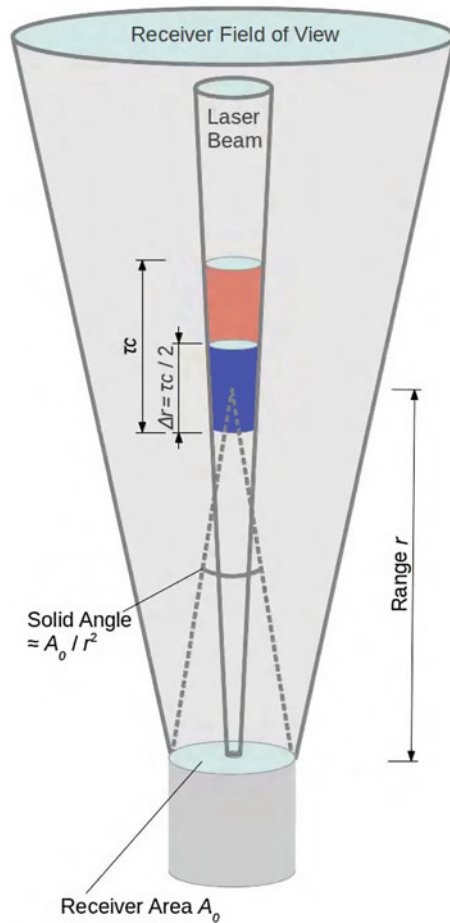


Fig. 2.4 Lidar geometry

detection efficiency. The value of P_0 determines the peak intensity of the backscatter cross section. A_0 determines the solid angle of the backscatter cross section that is subtended from a given range as shown in Fig. 2.4. The factor $\frac{c\tau}{2}$, also illustrated in Fig. 2.4, determines the range resolution of a pulsed system by establishing the time (distance) required for backscattered light from the beginning of the pulse to meet the forward-propagating light from the end of the pulse. Typically τ and A_0 are well characterised, P_0 may be known but is often prone to variability, and η can usually only be estimated to varying degrees of accuracy depending upon the complexity of the system and understanding of the efficiency of each component. Because of this uncertainty, it is often desirable to find a way to process lidar using a method that allows dependence on specific knowledge of the system constant to be cancelled out.

2.5 The Single-Scattering Elastic Lidar Equation

In the case where molecular returns are negligible compared to aerosol returns, which is the realm most relevant to ceilometer measurements, the range-dependent backscatter and extinction coefficients can be considered as functions only of the aerosol and water droplet returns. Under the assumption of single-scattering, and if a discrete laser wavelength is used, the lidar equation in this case can be expressed in the form [12]

$$P(r) = K_s \beta(r) \frac{O(r)}{r^2} e^{-2 \int_0^r \alpha(r') dr'}, \quad (2.16)$$

where $P(r)$ is the power detected from range r , K_s is the system constant given in Eq. 2.15, $\beta(r)$ is the scattering coefficient from the scattering volume at range r , $O(r)$ is the overlap function which describes what fraction of the laser beam cross section at a given range will be imaged onto the detector (this function reaches a value of unity at a full overlap distance r_0), $\frac{1}{r^2}$ is the range dependence factor that accounts for the decrease in solid angle subtended with the square of the range, and the remaining factor, $e^{-2 \int_0^r \alpha(r') dr'}$, based on the range dependent extinction coefficient $\alpha(r)$, is the integrated two-way extinction of the signal as it propagates from the instrument to the scattering volume at range r and back.

2.6 Elastic Lidar Inversion

A number of approaches for the inversion of elastic lidar signals have been described in the literature. Each of these methods applies a different set of assumptions in order to achieve inversion. While there are a variety of alternatives to, variations on, and combinations of these techniques (for example, [19, 20]) as well as detailed error analyses (for example, [21, 22]), only the fundamental methods are discussed here.

2.6.1 Slope Method

The first lidar inversion method described in the literature was the slope method discussed in 1966 by Collis [23]. In homogeneous atmospheric conditions, the extinction and backscatter coefficients can be assumed to be constants. In this case, the natural logarithm of the range-corrected lidar return is linear and from its slope the extinction coefficient can be derived. Kovalev and Eichinger note that in order to satisfy the homogeneity requirement the atmosphere need not be purely homogeneous but rather that local inhomogeneities do not significantly alter the linear fit across the region of interest [11]. They explain that for homogeneous atmospheres this method is often the best way to extract mean aerosol extinction, particularly if the aerosol and molecular returns are of similar amplitude. Kovalev and Eichinger caution, however, that if returns from aerosol-free atmospheres are being processed by this method, care must be taken to fully account for any background noise on the signal as that can greatly affect the slope that is calculated. They also emphasise the importance of either disregarding the region of incomplete overlap of the transmitter and receiver or carefully compensating for it.

2.6.2 Close Boundary Solution

A close boundary solution applies an assumed or measured value of the extinction coefficient at the start of the measurement range and inverts the signal in the forward direction. This method was first applied to lidar in 1967 by Barrett and Ben-Dov [24]. It can be applied successfully in clear atmospheric conditions, but in turbid conditions it quickly becomes unstable due to its mathematical formulation; its performance can be improved somewhat, however, by placing constraints that limit the possible solutions to positive values of extinction without extremely large “runaway” values [25].

2.6.3 Optical Depth Solution

Another approach to inversion, first introduced in 1988 by Weinman [26], is the optical depth solution. If the total optical depth of a lidar measurement range can be estimated, the transmission term in the lidar equation can be determined; this then acts as a constraint for the inversion. An important calibration method described in Sect. 2.8 is related to this approach. In order to perform an inversion based on the optical depth solution for combined molecular-aerosol atmospheres, three inputs typically used are the sun photometer-derived aerosol optical depth, the profile of molecular extinction (this may be disregarded if aerosol extinction is much greater than molecular extinction at the laser wavelength), and an aerosol lidar ratio assumption relating backscatter to extinction [27].

2.6.4 Far Boundary Solution

The most widely used method for inverting elastic lidar returns is the backward inversion method. This method, though also developed in similar form independently by Kaul in 1977 [28] and Zuev in 1978 [29]—those studies were not accessible in Western countries at the time—is typically credited to Klett who introduced it in 1981 [18]. In this method the extinction coefficient at the far boundary is assumed and the signal is inverted backward toward the instrument. This approach provides a stable result provided there are considerable aerosol or cloud returns present and is therefore the method typically applied in the inversion of ceilometer returns. The contemporary version of Klett’s approach was reformulated in 1982 by Fernald [30], and a method for improving the lidar ratio assumption and a smoothing process at the boundary point were described in 1984 by Sasano and Nakane [31]. It is therefore sometimes referred to as the Klett-Fernald-Sasano inversion, however, in this thesis it is simply referred to as the Klett inversion.

The Klett inversion requires an input value of the extinction coefficient at the far boundary of the lidar range. This boundary value can be measured or assumed. Since information from in situ measurement of the extinction coefficient at the far range of the instrument is not usually available for vertical lidar profiling, boundary extinction is typically assumed from some knowledge of the current atmospheric conditions.

2.6.5 Derivation of the Far Boundary Solution

Under the assumption of a single-component atmosphere, in which aerosol returns dominate molecular returns (reasonable for ceilometers at 905 nm), the far-boundary solution can be derived in a straightforward manner following the approach of Kovalev and Eichinger [11]. The lidar equation can first be rewritten somewhat by removing the overlap dependence. Overlap and its correction are discussed in detail in Chaps. 3 and 4, but here only ranges beyond the full overlap height r_0 are considered such that $O(r) = 1$. Equation 2.16 therefore becomes

$$P(r) = K_s T_{r_0}^2 \frac{\beta(r)}{r^2} e^{-2 \int_{r_0}^r \alpha(r') dr'}, \quad (2.17)$$

where $T_{r_0}^2$ is a constant accounting for the unknown transmittance from $r = 0$ to $r = r_0$.

If the lidar ratio is introduced as in Eq. 2.13, the backscatter coefficient $\beta(r)$ can be expressed in terms of extinction $\alpha(r)$ and lidar ratio function $\Pi_p(r)$ allowing Eq. 2.17 to be rewritten as

$$P(r) = K_s T_{r_0}^2 \frac{\Pi_p(r) \alpha(r)}{r^2} e^{-2 \int_{r_0}^r \alpha(r') dr'}. \quad (2.18)$$

Assuming that the particles along the measurement range are similar to each other, the backscatter to extinction ratio can be expressed by the constant Π_p such that

$$\Pi_p(r) = \Pi_p. \quad (2.19)$$

Kovalev and Eichinger note that if the variation among scatterers is relatively small, this assumption is reasonable, but that if precise determination of extinction is required, it can be problematic. If the assumption is applied, the unknown parameters of the measurement can now be expressed as a single constant such that

$$K_L = K_s T_{r_0}^2 \Pi_p, \quad (2.20)$$

and Eq. 2.18 can be written as

$$P(r) = K_L \frac{\alpha(r)}{r^2} e^{-2 \int_{r_0}^r \alpha(r') dr'}. \quad (2.21)$$

If $Z(r)$, the range-corrected signal, is considered, where $Z(r) = P(r)r^2$, then

$$Z(r) = K_L \alpha(r) e^{-2 \int_{r_0}^r \alpha(r') dr'}. \quad (2.22)$$

If the extinction coefficient $\alpha(r_b)$ at the far boundary r_b is known or can be estimated, the constant K_L can be written

$$K_L = \frac{Z(r_b)}{\alpha(r_b) e^{-2 \int_{r_0}^{r_b} \alpha(r') dr'}}. \quad (2.23)$$

Substituting this into Eq. 2.22, the range-corrected signal becomes

$$Z(r) = \frac{Z(r_b) \alpha(r) e^{-2 \int_{r_0}^r \alpha(r') dr'}}{\alpha(r_b) e^{-2 \int_{r_0}^{r_b} \alpha(r') dr'}}. \quad (2.24)$$

If this is expressed as the ratio of range corrected signal $Z(r_b)$ at the boundary r_b to the extinction coefficient $\alpha(r_b)$ at the boundary,

$$\frac{Z(r_b)}{\alpha(r_b)} = \frac{Z(r)}{\alpha(r)} \frac{e^{-2 \int_{r_0}^{r_b} \alpha(r') dr'}}{e^{-2 \int_{r_0}^r \alpha(r') dr'}}, \quad (2.25)$$

which can be rewritten as

$$\frac{Z(r_b)}{\alpha(r_b)} = \frac{Z(r)}{\alpha(r)} e^{-2 \int_r^{r_b} \alpha(r') dr'}. \quad (2.26)$$

By solving this equation for $Z(r)$ and integrating both sides over the interval r to r_b , an expression for the transmission term, $e^{-2 \int_r^{r_b} \alpha(r') dr'}$, can be derived in the form

$$e^{-2 \int_r^{r_b} \alpha(r') dr'} = 1 + \frac{\alpha(r_b)}{Z(r_b)} \left[2 \int_r^{r_b} Z(r') dr' \right]. \quad (2.27)$$

If this is substituted into Eq. 2.26 and $\alpha(r)$ is solved for, the Klett solution is arrived at such that

$$\alpha(r) = \frac{Z(r)}{\frac{Z(r_b)}{\alpha(r_b)} + 2 \int_r^{r_b} Z(r') dr'}. \quad (2.28)$$

In this way the range-dependent extinction coefficient is expressed in terms of only the range-corrected signal and the boundary value of the extinction coefficient.

This solution is useful because even though it relies on an assumed boundary condition at the far boundary, it is stable in the near-range due to the fact that the factor $2 \int_r^{r_b} Z(r') dr'$ increases with decreasing r . In addition, as ranges closer and closer to the instrument are considered, errors due to incorrect assumption of the far boundary condition reduce significantly due to the reduced influence of the factor $\frac{Z(r_b)}{\alpha(r_b)}$, particularly in turbid atmospheres [18]. This far boundary solution is applied in Chap. 5 in order to invert prototype lidar returns.

2.6.6 Boundary Condition Selection for Klett Inversion

There are two factors to consider when making the far-range boundary assignment. The first of these is the signal level. Usually the maximum possible measurement range is desirable. In this case, the boundary condition is assigned at the farthest point in the signal that is above a certain threshold. Two examples of this from the literature are 2.3 % of the maximum digitised signal amplitude [32], assuming the dynamic range of the receiver electronics is appropriately matched to the dynamic range of the signals, or, in another work, a signal to noise ratio of 5–10 dB [33]. Choosing a boundary point too close to the noise level is likely to reduce the accuracy of the inversion. A signal to noise ratio method for locating the boundary range is applied in Chap. 5.

The second factor to consider is the boundary value of the extinction coefficient. It is possible to estimate the boundary value of the extinction coefficient directly from the signal by considering the slope of the logarithmic range-corrected signal as explained by Klett [18], such that

$$\alpha_b \approx \frac{\ln [P(r_s) r_s^2] - \ln [P(r_b) r_b^2]}{2(r_b - r_s)}. \quad (2.29)$$

This is calculated over a region starting at a selected range r_s and reaching to the maximum range r_b at the boundary. This method works best over a homogeneous region with significant returns.

If no clearly homogeneous region is present, a default value can be used depending upon measurement conditions. While a clear air value such as 10^{-4} m^{-1} can be applied as in [34], for cloud detection applications it may be better to select a cloud value such as $0.02 \cdot 10^{-4} \text{ m}^{-1}$ as in [32], particularly if it is unlikely that clear air can be detected at far ranges or beyond a cloud layer due to attenuation and lack of sensitivity. Kovalev and Eichinger state that if the effects of multiple scattering are small, it is straightforward to assign a boundary value $\alpha(r_b)$ within a cloud. This approach is generally applicable to ceilometers, both because of their limited sensitivity to molecular returns and because their primary function is cloud detection, and is applied in Chap. 5.

2.6.7 Stability of the Klett Inversion

A few examples of the behaviour of the Klett inversion under various conditions illustrate its value. First, Fig. 2.5 shows the influence on the inversion of overestimating or underestimating the boundary value of the extinction coefficient by 50 %. In both cases the inversion converges on the correct profile quite quickly as the range is considered backwards from the boundary r_b toward $r = 0$. Second, Fig. 2.6 shows the influence of incorrect assumption of the lidar ratio exponent k from Eq. 2.14. While the inversion is certainly sensitive to the lidar ratio exponent, it still strays in this case by less than 40 % at most from the correct value, which is not much considering that values of the extinction coefficient range over several orders of magnitude. Finally,

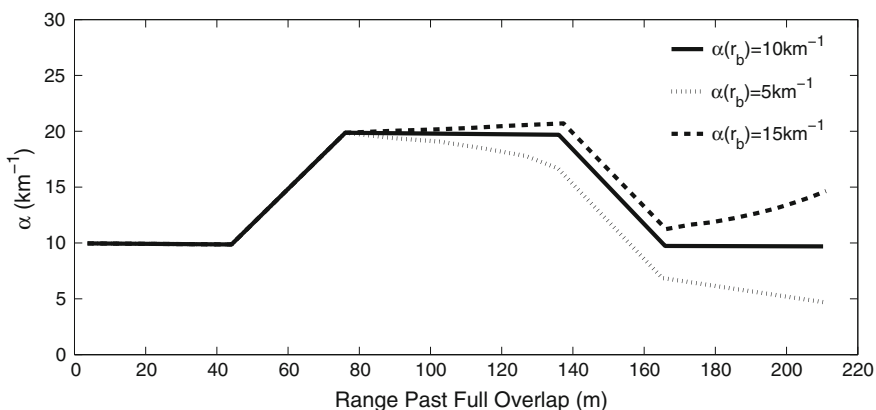


Fig. 2.5 Influence of boundary extinction value $\alpha(r_b)$ on backward inversion as originally calculated by Klett [18]

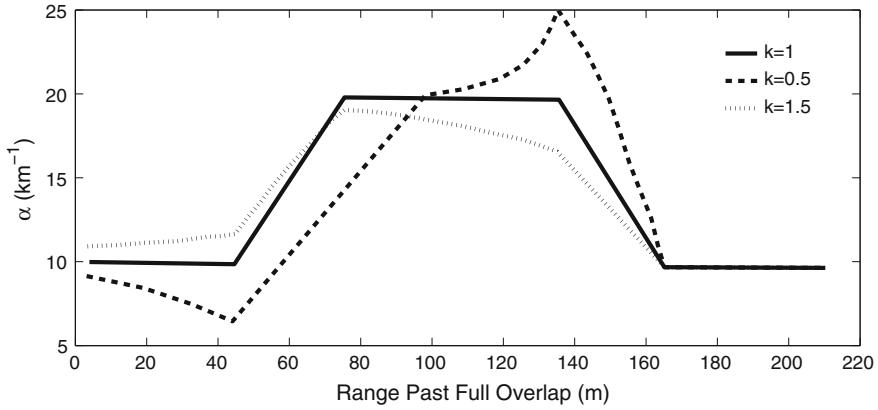


Fig. 2.6 Influence of lidar ratio exponent k on backward inversion as originally calculated by Klett [18]

since range-corrected signals are typically noisy at far ranges, the influence of this noise on inversion also needs to be considered. A thorough examination of error sensitivity of the backward inversion technique has been given by Rocadenbosch and Comerón [22].

2.7 Attenuated Backscatter

Since inverted data depends greatly on the inversion technique, the inverted profile is often not the best profile for inter-comparison of different instruments. The profile used most widely for instrument comparison is the attenuated backscatter, that is, the range-corrected, overlap-corrected, calibrated signal. It is a standard output of satellite lidar data [35] and is also a typical ceilometer output.

Considering discussion in [35, 36], attenuated backscatter $\beta'(r)$ can be expressed, by solving the lidar equation for the product of backscatter and transmission, as

$$\beta'(r) = \frac{P(r)r^2}{K_s O(r)} = \beta(r) T_{\text{tot}}^2(r), \quad (2.30)$$

where T_{tot} is the total transmission through all scatterers. The range-corrected power $P(r)r^2$ divided by the product of the overlap function $O(r)$ and the system constant K_s therefore reflects the combined contributions of backscatter and attenuation. By fully expressing the system constant K_s using Eq. 2.15, the attenuated backscatter becomes

$$\beta'(r) = \frac{P(r)r^2}{P_0 \frac{\tau_c}{2} O(r) A_0}, \quad (2.31)$$

given throughout this thesis in units of $\text{m}^{-1} \text{sr}^{-1}$.

2.8 Calibration of Attenuated Backscatter

One problem with the attenuated backscatter output is its dependence on knowledge of the transmitted laser power P_0 and the calibrated received power $P(r)$, which are often poorly characterised and/or variable in a lidar system. In order to overcome this problem, O'Connor et al. devised a calibration method [37] that uses returns from fully signal-attenuating stratocumulus water clouds, whose optical scattering properties are well understood, to calibrate the attenuated backscatter output of an elastic lidar system.

The transmission T_{tot} in Eq. 2.30 is dominated in this case by returns from the cloud droplets and can be expressed by application of Eq. 2.11 as

$$T_{\text{tot}}(r) = e^{-\int_0^r \alpha(r')dr'} = e^{-\tau_\alpha}, \quad (2.32)$$

where, as previously noted, the integrated extinction $\int_0^r \alpha(r)dr$ is equivalent to the optical depth, τ_α . Equation 2.30 can therefore be rewritten

$$\beta'(r) = \beta(r)e^{-2\tau_\alpha}. \quad (2.33)$$

Instead of defining the lidar ratio as the backscatter to extinction ratio $\Pi_p = \frac{\beta}{\alpha}$, O'Connor et al. used the extinction to backscatter ratio and defined it as $S = \frac{\alpha}{\beta}$. Assuming an infinitesimal change dr in range, for the single scattering case the corresponding change $d\tau_\alpha$ in optical depth can be expressed as

$$d\tau_\alpha = S(r)\beta(r)dr. \quad (2.34)$$

A factor, $\eta_m(r)$, that corrects for multiple scattering effects and ranges from 0.5 to 1 can then be introduced such that

$$d\tau_\alpha = \eta_m(r)S(r)\beta(r)dr. \quad (2.35)$$

If the attenuated backscatter as stated in Eq. 2.33 is integrated over the entire range of the instrument, the resulting value B is expressed

$$B = \int_0^\infty \beta'(r)dr = \int_0^\infty \beta(r)e^{-2\tau_\alpha}dr. \quad (2.36)$$

If Eq. 2.35 is substituted into this expression and η_m and S are assumed constant, it becomes

$$B = \int_0^\infty \beta'(r)dr = \frac{1}{\eta_m S} \int_0^\infty e^{-2\tau_\alpha} d\tau_\alpha. \quad (2.37)$$

Since the integral $\int_0^\infty e^{-2\tau_\alpha} d\tau_\alpha$ can be evaluated such that

$$\int_0^\infty e^{-2\tau_\alpha} d\tau_\alpha = \frac{1}{2}, \quad (2.38)$$

the integrated attenuated backscatter becomes

$$B = \int_0^\infty \beta'(r) = \frac{1}{2\eta_m S}, \quad (2.39)$$

and the attenuated backscatter calibration should be adjusted until this is true.

O'Connor et al. specified that the stratocumulus cloud used for calibration must have a peak backscatter coefficient of greater than $1 \times 10^{-4} \text{ sr}^{-1}$ and the signal level at this height must be at least 20 times greater than that 300 m above. In addition, no precipitation or strong aerosol events should be present during calibration. Using a droplet size spectrum width parameter (μ) ranging from 2 to 10, and median droplet diameters ($2 \times a_0$) between 4 and $10 \mu\text{m}$ to define the droplet size distribution in a thick stratocumulus cloud, they derived an effective lidar ratio of $S = 18.8 \pm 0.8 \text{ sr}$ at 905 nm as the appropriate lidar ratio for this technique. The multiple scattering correction factor η_m is discussed further in Chap. 5 where this method is applied.

This calibration technique provides a useful means of calibrating the signal output from an instrument whose system parameters may be poorly characterised or subject to drift.

2.9 Conclusion

This chapter has discussed fundamental theoretical tools used to describe the nature of scattering particles in clouds and the mechanics of elastic scattering in the atmosphere. It has introduced the single-scattering elastic lidar equation and the parameters it contains, including the geometry involved. It has presented a derivation of the classical backward inversion technique used in elastic lidar and shown its robustness. Finally, it has explained the attenuated backscatter function used for inter-comparison of lidar returns along with a method by which it can be calibrated. The geometry of lidar measurement has largely guided the design of the prototype described in Chap. 3. The lidar equation is applied in a variety of ways in Chaps. 3, 4 and 5, and inversion and calibration both become important in Chap. 5.

References

1. H. Pruppacher, J. Klett, *Microphysics of Clouds and Precipitation* (Kluwer Academic Publishers, Dordrecht, 1997)
2. D. Deirmendjian, *Electromagnetic Scattering on Spherical Polydispersions* (American Elsevier Pub. Co., RAND Corporation, New York, 1969)
3. M. Abramowitz, I. Stegun, *Handbook of Mathematical Functions: with Formulas, Graphs, and Mathematical Tables*, Applied mathematics series (Dover Publications, New York, 1964)
4. A. Kokhanovsky, Optical properties of terrestrial clouds. *Earth Sci. Rev.* **64**(34), 189–241 (2004)
5. B. Mason, *Clouds, Rain and Rainmaking* (Cambridge University Press, Cambridge, 1975)
6. Q. Han, W.B. Rossow, A.A. Lacis, Near-global survey of effective droplet radii in liquid water clouds using ISCCP data. *J. Clim.* **7**(4), 465–497 (1994)
7. B. Fomin, I. Mazin, Model for an investigation of radiative transfer in cloudy atmosphere. *Atmos. Res.* **4748**(0), 127–153 (1998)
8. R. Knollenberg, Clouds, their formation, optical properties, and effects, ser. *Techniques for Probing Cloud Microstructure*, *Academic Press Rapid Manuscript Reproduction* (Academic Press, San Diego, 1981), pp. 15–92
9. P. Hobbs, A. Deepak, Clouds, their formation, optical properties, and effects, ser. *Academic Press Rapid Manuscript Reproduction*, ed. by P. Hobbs, A. Deepak (Academic Press, San Diego, 1981).
10. D.K. Lynch, K. Sassen, D.O. Starr, G. Stephens (eds.), *Cirrus* (Oxford University Press, New York, 2002)
11. V. Kovalev, W. Eichinger, *Elastic Lidar: Theory, Practice, and Analysis Methods* (John Wiley and Sons Inc, Hoboken, 2004)
12. U. Wandinger, “Introduction to lidar”, in *LIDAR: range-resolved optical remote sensing of the atmosphere*, ed. by C. Weitkamp (Springer, New York, 2005), pp. 1–18
13. G. Mie, Beiträge zur optik trüber medien, speziell kolloidaler metallösungen. *Ann. Phys.* **330**(3), 377–445 (1908)
14. S. Prah, Mie scattering calculation. (Oregon Medical Laser Center), http://omlc.ogi.edu/calc/mie_calc.html. Accessed July 2012
15. W.J. Smith, *Modern Optical Engineering* (SPIE, New York, 2008)
16. E.W. Eloranta, Practical model for the calculation of multiply scattered lidar returns. *Appl. Opt.* **37**(12), 2464–2472 (1998)
17. G.M. Hale, M.R. Querry, Optical constants of water in the 200-nm to 200- μm wavelength region. *Appl. Opt.* **12**(3), 555–563 (1973)
18. J.D. Klett, Stable analytical inversion solution for processing lidar returns. *Appl. Opt.* **20**(2), 211–220 (1981)
19. F. Rocadenbosch, C. Soriano, A. Comerón, J.-M. Baldasano, Lidar inversion of atmospheric backscatter and extinction-to-backscatter ratios by use of a Kalman filter. *Appl. Opt.* **38**(15), 3175–3189 (1999)
20. I.S. Stachlewska, C. Ritter, On retrieval of lidar extinction profiles using two-stream and Raman techniques. *Atmos. Chem. Phys.* **10**(6), 2813–2824 (2010)
21. F. Rocadenbosch, A. Comerón, D. Pineda, Assessment of lidar inversion errors for homogeneous atmospheres. *Appl. Opt.* **37**(12), 2199–2206 (1998)
22. F. Rocadenbosch, A. Comerón, Error analysis for the lidar backward inversion algorithm. *Appl. Opt.* **38**(21), 4461–4474 (1999)
23. R. Collis, Lidar: a new atmospheric probe. *Q.J.R. Meteorol. Soc.* **92**, 220–230 (1966)
24. E.W. Barrett, O. Ben-Dov, Application of the lidar to air pollution measurements. *J. Appl. Meteorol.* **6**, 500–515 (1967)
25. V.A. Kovalev, H. Moosmüller, Distortion of particulate extinction profiles measured with lidar in a two-component atmosphere. *Appl. Opt.* **33**(27), 6499–6507 (1994)
26. J.A. Weinman, Derivation of atmospheric extinction profiles and wind speed over the ocean from a satellite-borne lidar. *Appl. Opt.* **27**(19), 3994–4001 (1988)

27. V.A. Kovalev, Stable near-end solution of the lidar equation for clear atmospheres. *Appl. Opt.* **42**(3), 585–591 (2003)
28. B. Kaul, Laser sensing the aerosol pollution in the atmosphere, Ph.D. dissertation, Institute of Atmospheric Optics, Tomsk, 1977
29. V. Zuev, G. Zadde, S. Kavkjanov, B. Kaul, Interpretation of Lidar Signals from the Regions of Large Optical Depths, *Remote Sensing of the Atmosphere* (Nauka, Novosibirsk, 1978), pp. 60–68
30. F.G. Fernald, in *proceedings, in Eleventh International Laser Radar Conference* (Madison, Wisc, 1982), p. 213
31. Y. Sasano, H. Nakane, Significance of the extinction/backscatter ratio and the boundary value term in the solution for the two-component lidar equation. *Appl. Opt.* **23**(1), 11–13 (1984)
32. W. Carnuth, R. Reiter, Cloud extinction profile measurements by lidar using klett's inversion method. *Appl. Opt.* **25**(17), 2899–2907 (1986)
33. J. Dias, J. Leita, E. Fonseca, Reconstruction of backscatter and extinction coefficients in lidar: a stochastic filtering approach. *IEEE Trans. Geosci. Remote Sens.* **42**(2), 443–456 (2004)
34. J.L. Gaumet, J.C. Heinrich, M. Cluzeau, P. Pierrard, J. Prieur, Cloud-base height measurements with a single-pulse erbium-glass laser ceilometer. *J. Atmos. Oceanic Technol.* **15**(1), 37–45 (1998)
35. M. Vaughan, S. Young, D. Winker, K. Powell, A. Omar, Z. Liu, Y. Hu, C. Hostetler, Fully automated analysis of space-based lidar data: an overview of the CALIPSO retrieval algorithms and data products, in *Laser Radar Techniques for Atmospheric Sensing, Proceedings of SPIE*, vol. 5575, 2004
36. L. Mona, A. Amodeo, G. D'Amico, G. Pappalardo, First comparisons between CNR-IMAA multi-wavelength Raman lidar measurements and CALIPSO measurements. in *Lidar Technologies, Techniques, and Measurements for Atmospheric Remote Sensing III*, eds. by U. Singh, G. Pappalardo. ser. Proceedings of SPIE-the International Society for Optical Engineering, SPIE, 2007 (Florence, Italy, 2007), pp. 675 010-1–675 010-10
37. E. O'Connor, A. Illingworth, R. Hogan, A technique for autocalibration of cloud lidar. *J. Atmos. Oceanic Technol.* **21**, 777–786 (2004)

A Novel Lidar Ceilometer

Design, Implementation and Characterisation

Vande Hey, J.D.

2015, XIX, 158 p. 73 illus., 10 illus. in color., Hardcover

ISBN: 978-3-319-12612-8